ISSN 1674-1056
http://cpb.iphy.ac.cn
http://iopscience.iop.org/cpb
中国物理 B
Chinese Physics
中国物理 Chinese Physics B

Qubits based on semiconductor quantum dots

Xin Zhang(张鑫), Hai-Ou Li(李海欧), Ke Wang(王柯), Gang Cao(曹刚), Ming Xiao(肖明), Guo-ping Guo(郭国平)
Citation: Chin. Phys. B . 2018, 27(2): 020305. **doi:** 10.1088/1674-1056/27/2/020305

Journal homepage: http://cpb.iphy.ac.cn; http://iopscience.iop.org/cpb

What follows is a list of articles you may be interested in

Novel quantum watermarking algorithm based on improved least significant qubit modification for quantum audio

Zhi-Guo Qu(瞿治国), Huang-Xing He(何煌兴), Tao Li(李涛)
Chin. Phys. B . 2018, 27(1): 010306. **doi:** 10.1088/1674-1056/27/1/010306

Invariants-based shortcuts for fast generating Greenberger—Horne—Zeilinger state among three superconducting qubits

Jing Xu(徐晶), Lin Yu(于琳), Jin-Lei Wu(吴金雷), Xin Ji(计新)
Chin. Phys. B . 2017, 26(9): 090301. **doi:** 10.1088/1674-1056/26/9/090301

Superconducting phase qubits with shadow-evaporated Josephson junctions

Fei-Fan Su(宿非凡), Wei-Yang Liu(刘伟洋), Hui-Kai Xu(徐晖凯), Hui Deng(邓辉), Zhi-Yuan Li(李志远), Ye Tian(田野), Xiao-Bo Zhu(朱晓波), Dong-Ning Zheng(郑东宁), Li Lv(吕力), Shi-Ping Zhao(赵士平)
Chin. Phys. B . 2017, 26(6): 060308. **doi:** 10.1088/1674-1056/26/6/060308

Fast generating *W* state of three superconducting qubits via Lewis-Riesenfeld invariants

Lin Yu(于琳), Jing Xu(徐晶), Jin-Lei Wu(吴金雷), Xin Ji(计新)
Chin. Phys. B . 2017, 26(6): 060306. **doi:** 10.1088/1674-1056/26/6/060306

Creating nitrogen–vacancy ensembles in diamond for coupling with flux qubit

Ya-Rui Zheng(郑亚锐), Jian Xing(邢健), Yan-Chun Chang(常彦春), Zhi-Guang Yan(闫智广), Hui Deng(邓辉), Yu-Lin Wu(吴玉林), Li Lü(吕力), Xin-Yu Pan(潘新宇), Xiao-Bo Zhu(朱晓波), Dong-Ning Zheng(郑东宁)
Chin. Phys. B . 2017, 26(2): 020305. **doi:** 10.1088/1674-1056/26/2/020305

TOPICAL REVIEW — Solid-state quantum information processing

Qubits based on semiconductor quantum dots*

Xin Zhang(张鑫), Hai-Ou Li(李海欧)†, Ke Wang(王柯), Gang Cao(曹刚), Ming Xiao(肖明), and Guo-Ping Guo(郭国平)‡

Key Laboratory of Quantum Information, Chinese Academy of Sciences, University of Science and Technology of China, Hefei 230026, *China*

(Received 3 September 2017; revised manuscript received 19 December 2017; published online 5 January 2018)

Semiconductor quantum dots are promising hosts for qubits to build a quantum processor. In the last twenty years, intensive researches have been carried out and diverse kinds of qubits based on different types of semiconductor quantum dots were developed. Recent advances prove high fidelity single and two qubit gates, and even prototype quantum algorithms. These breakthroughs motivate further research on realizing a fault tolerant quantum computer. In this paper we review the main principles of various semiconductor quantum dot based qubits and the latest associated experimental results. Finally the future trends of those qubits will be discussed.

Keywords: semiconductor quantum dot, qubit, quantum computing, cavity quantum electrodynamics

PACS: 03.67.Lx, 03.67.–a, 68.65.Hb, 78.67.Hc **DOI:** 10.1088/1674-1056/27/2/020305

1. Introduction

Quantum computers that directly use the principles of quantum mechanics to perform operations on data are believed to have great potential across a vast range of applications, from cryptography, big data, scientific simulation to even machine learning and artificial intelligence. In these fields, quantum computers would crack problems inaccessible to even the largest classical supercomputer today (such as China's Sunway TaihuLight), which is called 'quantum supremacy'. Therefore, to master the new technology in the foreseeable future, building a quantum computer becomes one core issue in today's research.

The basic difference between quantum computers and their classical counterparts is that quantum computers are built on qubits rather than bits. Up to now, many different physical realizations of qubits have been proposed experimentally, including superconducting circuits,[1,2] trapped ions,[3] donors in silicon,[4] semiconductor quantum dots,[5,6] etc. Among them semiconductor quantum dots are most promising considering that their fabrication process is most compatible with standard CMOS (complementary metal–oxide–semiconductor) technology. In the past 20 years, qubits based on different degrees of electrons or holes in quantum dots have been developed, including charge states of electrons,[7] spin states of an electron[8] or hole,[9] singlet-triplet states of two electrons,[10] and other hybrid states.[11,12] Here we first introduce the concept of semiconductor quantum dots, then we present different types of qubits and give the most recent progress, and finally the future trends of those qubits are discussed.

2. Semiconductor quantum dots

The semiconductor quantum dot is also called 'artificial atom', which is a three dimensional potential well formed inside a semiconductor that can trap a few or even a single electron. Materials mostly used for the quantum dots are GaAs and Si. Due to the high mobility of electrons in GaAs/AlGaAs heterostructure, GaAs was the first material to host qubits based on quantum dots.[13–15] As illustrated in Fig. 1(a), the electrodes on the surface of GaAs offer voltage to form a potential well for trapping electrons in the two-dimensional electron gas (2DEG). Readout of charge states can be realized either by transport current $I_{\rm dot}$ from source to drain or by the current $I_{\rm QPC}$ of a quantum point contact (QPC). QPC measurement was proved to be more sensitive than transport measurement. The conductivity of a QPC can change dramatically when an electron tunnels into or out of the quantum dot, leading to the observation of a single electron regime in a quantum dot.

Compared to GaAs, silicon is an excellent host material for spin qubits, for its weak hyperfine interaction and spin–orbit coupling[16] that reduce the magnetic noise. A silicon quantum dot can be formed either in the Si well of an Si/SiGe heterostructure or in a CMOS channel. The Si/SiGe quantum dot can be divided into two categories: the doped Si/SiGe quantum dot and the undoped Si/SiGe quantum dot. The doped type is similar to GaAs quantum dots shown in Fig. 1(a), where the electrons forming 2DEG are supplied by the doped layer,[17] however, the doped heterostucture introduces charging noise from the doped layer and thus was replaced gradually by the undoped heterostructure, which uses a global gate on top of an insulating layer to introduce electrons in the Si

*Project supported by the National Key Research and Development Program of China (Grant No. 2016YFA0301700), the National Natural Science Foundation of China (Grant Nos. 61674132, 11674300, 11575172, and 11625419), and the Fundamental Research Fund for the Central Universities.

†Corresponding author. E-mail: haiouli@ustc.edu.cn

‡Corresponding author. E-mail: gpguo@ustc.edu.cn

© 2018 Chinese Physical Society and IOP Publishing Ltd

well.[18] As shown in Fig. 1(b), the gates for quantum dot formation like traditional GaAs quantum dots are beneath the insulating layer. Inspired by this new architecture, recently, undoped GaAs quantum dots were also fabricated[19,20] to suppress noise. On the other hand, in the past few years, silicon CMOS quantum dots have developed rapidly since the structure of surface-top gates[21] was replaced by overlapping gates[22] for more tunable control. A scanning electron microscope (SEM) image of one overlapping-gate device fabricated in our laboratory is shown in Fig. 1(c), the upper half of the device is a single electron transistor (SET) serving as a charge sensor like a QPC channel while the lower half is a single quantum dot. The lead gates (green) introduce electrons from source and drain, and the SET is formed by two barrier gates (orange) while the quantum dot is formed by confinement gates (blue), plunger gates (red) and barrier gates (orange). As illustrated in Fig. 1(d), those gates for different uses overlap one another with a thin insulating oxide(sliver gray) in between for electrical isolating. Recently, such types of gates were also used in Si/SiGe quantum dots, and showed their potential for more flexible control.[23,24]

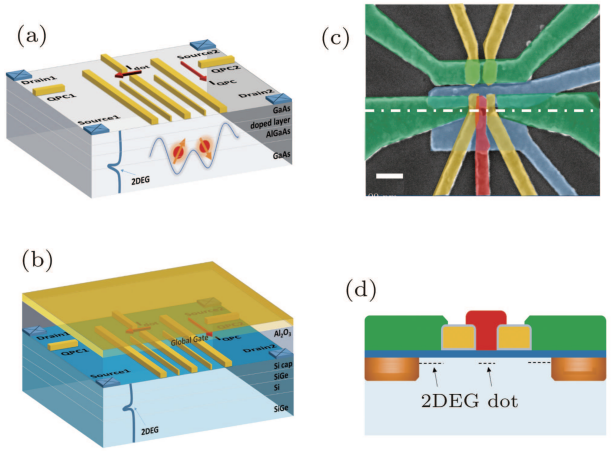


Fig. 1. (color online) Device structure of the semiconductor quantum dot. Panels (a) and (b) are schematics of a double quantum dot fabricated using doped AlGaAs/GaAs heterostructure and undoped Si/SiGe herterostructure, respectively. $I_{\rm dot}$ is the current from source to drain through the dot, while $I_{\rm QPC}$ is the current from source to drain through the QPC channel. The location of 2DEG and the electrons with spin directions in the double quantum dot are also shown. (c) Scanning electron micrograph (SEM) of a CMOS quantum dot with a SET as a charge sensor, where a white dash dotted line shows position of the cross section (d). Confinement gates (blue), lead gates (green), barrier gates (orange), and plunger gates (red) are shown. (d) Cross section of a CMOS quantum dot, dotted lines denote where 2DEG and a quantum dot form.

3. Qubits based on quantum dots

The quantum bit, also called a qubit, is a two-level quantum mechanical system that can be described by the Bloch sphere. In Fig. 2(a), the north and south pole of the Bloch sphere represent two basis states of the qubit, $|0\rangle$ and $|1\rangle$, respectively. However, different from classical bits, qubits can also reside in states of the linear combination of $|0\rangle$ and $|1\rangle$, which are called superposition states that occupy any point on the sphere. The operation of qubits requires that one can rotate the qubit on the sphere from one point to another arbitrarily. To achieve this goal, two-axis control of a qubit on the Bloch sphere is required. The axes for control are referred to as the x axis and z axis, respectively. The operation process is illustrated in Fig. 2(b).

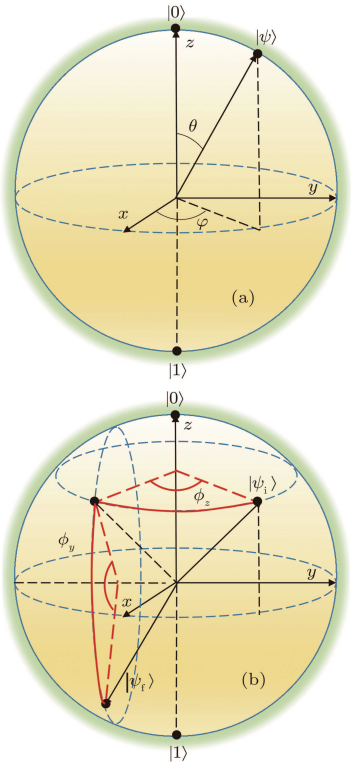


Fig. 2. (color online) Bloch sphere representation of a qubit. (a) State $|\psi\rangle$ is a superposition state of $|0\rangle$ and $|1\rangle$. (b) Single qubit gate operation shown in a Bloch sphere. Rotation from the initial state $|\psi_{\rm i}\rangle$ to the final state $|\psi_{\rm f}\rangle$ is finished by successive rotations around the z axis by ϕ_z and the y axis by $\phi_{\rm y}$.

There are two fundamental diagrams for characterizing a qubit based on quantum dots: charge stability diagram and engery level spectrum. These two kinds of diagrams for different types of qubits are depicted in Fig. 3. The charge stability diagram shows the charge occupancy tuned by the gate voltage. Except for the spin qubit that works only in a single dot, other types of qubits work in two or three dots, for which a variable named detuning ε that describes the electrochemical potential difference among different dots is introduced and denoted by the arrows in the charge stability diagrams. Detuning ε is of great significance when describing qubits because we use it to turn on or off a qubit in multiple dots, and thus in energy level spectrums the energy levels as a function of detuning are mostly depicted. Again, the spectrum for spin qubits is different because they rely on the magnetic field to control the energy level. The description of each diagram is detailed in the following subsections.

3.1. Charge qubit

Using the charge state of a double quantum dot is a direct way to form a qubit. The charge qubit is defined by the excess

electron occupation of the left dot or the right dot with electrochemical potentials $E_{\rm L}$ and $E_{\rm R}$. Here we denote $(N_{\rm l}, N_{\rm r})$ for the electron arrangement with $(0,1)$ $((1,0))$ representing the excess electron occupation of the right (left) dot and thus the basis state $|0\rangle$ $(|1\rangle)$. Detuning ε is defined as $\varepsilon \equiv E_{\rm R} - E_{\rm L}$, and the interdot tunneling gives an anticrossing gap $2t$. The effective Hamiltonian[7] is

$$H_C = \frac{1}{2}\varepsilon\sigma_z + t\sigma_x, \tag{1}$$

where σ_x and σ_z are the Pauli matrices for the bases of $|0\rangle$ and $|1\rangle$. As illustrated in the charge stability diagram of Fig. 3, when we use the surface gates to change the detuning ε, the eigenenergies, $E(1,0)$ and $E(0,1)$, will cross and an anticrossing appears. At the point $\varepsilon = 0$, the coherent oscillation around the z axis is expected with the angular frequency given by $\Omega = \sqrt{\varepsilon^2 + (2t)^2}/\hbar$. When ε does not equal to zero, the energy gap changes and a rotation around the x axis can be acquired. The universal control of the charge qubit was realized by Guo's group in GaAs quantum dots on the picosecond scale[25,26] in 2013, the probability of the qubit in the state $|1\rangle$ as a function of the driven pulse amplitude A, pulse length $t_{\rm p}$, and the energy position ε_0 is illustrated in Fig. 4. Later, Eriksson *et al*. demonstrated a charge qubit based on Si/SiGe quantum dots with two-axis control fidelities greater than 86%, which shows the promising future to realize quantum computing.[27]

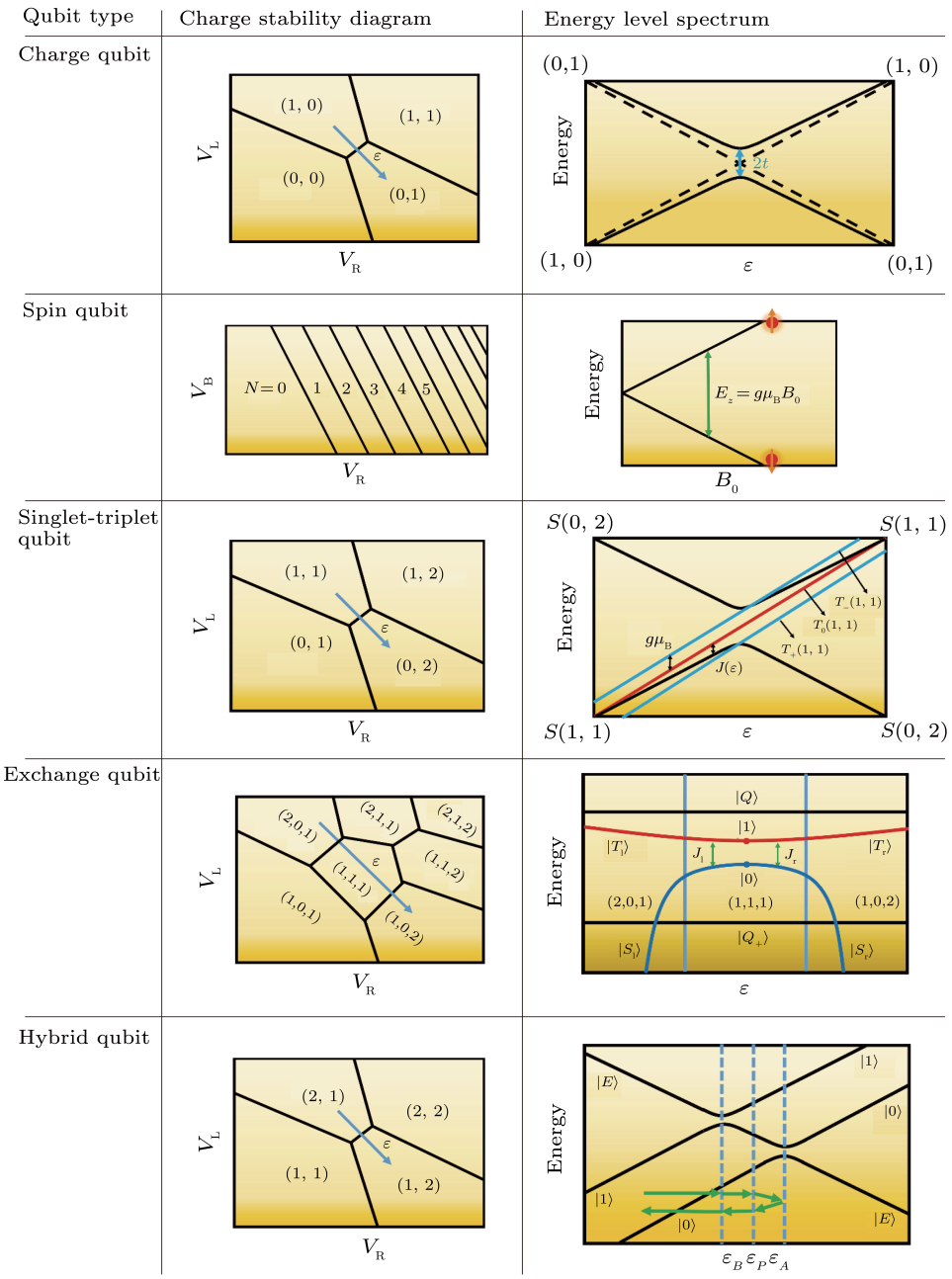


Fig. 3. (color online) Fundamental diagrams for different types of qubits. Charge stability diagrams are depicted by reading the information of charge occupancy as a function of gate voltage, in which '$V_{\rm L}$' ('$V_{\rm R}$') denote the gate that control the left (right) dot of a double quantum dot or the leftmost (rightmost) dot of a triple quantum dot, while '$V_{\rm B}$' ('$V_{\rm P}$') denote the barrier (plunger) gate that controls the single quantum dot. Energy level spectrums are depicted by analyzing the energy level as a function of detuning ε or the magnetic field $\boldsymbol{B}_0$.

Furthermore, the two qubit control of charge qubits can be realized by involving two double quantum dots coupled with energy J_c, which originates from the Coulomb repulsion between the electrons in each double quantum dot. The two-qubit Hamiltonian[28,29] can be written as

$$H_{\mathrm{TC}} = \sum_{i=1}^{2}\left(\frac{1}{2}\varepsilon_i\sigma_z^i + t_i\sigma_x^i\right) + \frac{J_c}{4}\sigma_z^1\otimes\sigma_z^2, \tag{2}$$

where ε_i and t_i refers to the detuning and anticrossing energy of the i-th quantum dot, respectively, while σ_z^i and σ_x^i denote the Pauli matrices of the i-th quantum dot. Shown by Fujisawa *et al.*,[28] various two-qubit gate operations can be performed by adjusting ε_1 and ε_2 with respect to J_c.

Many groups have tried to realize the two qubit gate of charge qubits experimentally. In 2009, Petersson *et al.* and Gou Shinkai *et al.* studied interactions between two capacitively coupled GaAs double quantum dots.[30,31] Later in 2015, Guo's group at USTC demonstrated conditional rotations of charge qubits using GaAs quantum dots with a clock speed up to 6 GHz[32] and the truth table of a Controlled-NOT (CNOT) gate is shown in Fig. 4. Furthermore, they also demonstrated controlled quantum operations in a triple qubit system recently.[33] Using quadruple Si/SiGe quantum dots, Eriksson's group also realized a conditional phase flip in 80 ps, demonstrating the potential for full demonstration of two qubit gates.[34]

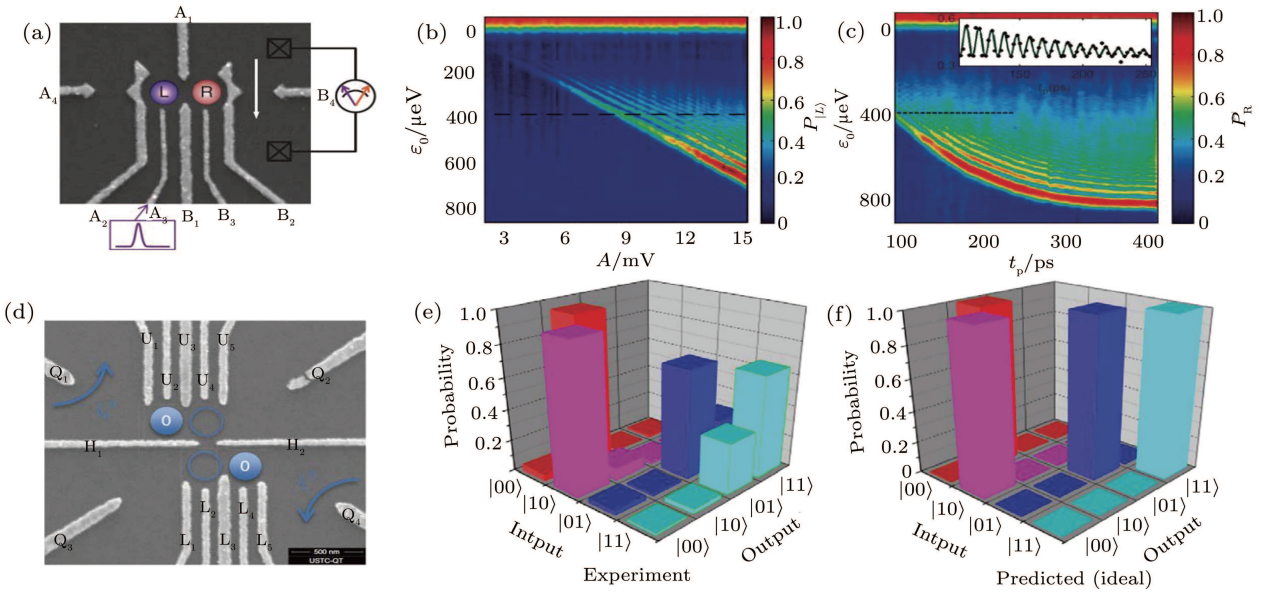


Fig. 4. (color online) Experimental demonstration of charge qubit gates.[25,32] Panels (a) and (d) are SEM images for the devices demonstrating one and two qubit gate operations, respectively. Quantum dots are denoted by circles and the I_{QPC} or G_{QPC} (the conductivity of QPC channel) are shown by arrows. Panels (b) and (c) show the probability of the qubit in the left dot state $P_{|L\rangle}$ as a function of the voltage amplitude A and the pulse width t_{p} at different detuning energy position ε_0, respectively. These results indicate that both the voltage amplitude and the pulse width can control the rotation to a certain angle at appropriate detuning points, leading to the universal control of charge qubits. The inset of panel (c) shows $P_{|L\rangle}$ along the line cut at $\varepsilon_0 = 400$ μeV, revealing ultrafast oscillations. Panels (e) and (f) demonstrate the truth table of CNOT operation experimentally and theoretically, respectively. $|mn\rangle$ denote the control qubit in the state $|n\rangle$ and the target qubit in the state $|m\rangle$. The red, pink, blue and green bars correspond to input states $|00\rangle$, $|10\rangle$, $|01\rangle$, and $|11\rangle$, respectively.

Though charge qubits have the advantage in qubit definition that all the operations can be achieved via electrodes with the manipulation rate reaching gigahertz, they are more sensitive to electric field fluctuations, which limits its decoherence time T_2^* dramatically, usually < 1 ns.[7,25,27,35] Decoherence time is one terminology of quantum mechanics that reflects the noise influence on a qubit and characterizes the time for a qubit to keep its quantum property, thus a short decoherence time will reduce the operation fidelity. To improve the fidelity, researches on analyzing charge noises should be propelled further.[27]

3.2. Spin qubit

Making use of a single electron spin as a qubit was first proposed by Loss and DiVincenzo in 1998.[8] Spin is a degree that reflects mostly the magnetic influence on a particle, thus spin qubits suffer less from charge noises compared to charge qubits and they usually possess much longer decoherence time. The basis states of spin qubits are two opposite spin directions that represent $|0\rangle$ and $|1\rangle$, respectively, split with Zeeman energy $E_z = g\mu_{\mathrm{B}}\boldsymbol{B}_0$ under a static magnetic field $\boldsymbol{B}_0$, where μ_{B} is the Bohr magneton and g the electron g factor. The Hamiltonian can be written as

$$H_{\mathrm{S}} = \frac{\hbar\omega_z}{2}\sigma_z, \tag{3}$$

where $\hbar\omega_z = g\mu_{\mathrm{B}}\boldsymbol{B}_0$, and the unitary time evolution of spin is defined by the operator $U(t) = R_z(\omega_z t)$. Consequently, a static field drives an electron spin rotating around the z axis and $\omega_z/2\pi$ is called Larmor frequency.[36]

Moreover, considering that single spin responds only to a magnetic field rather than an electric field, we still need electron spin resonance (ESR) or electric dipole spin resonance

(EDSR) to make the spin rotate around the x axis of the Bloch sphere. The ESR technique requires an oscillating magnetic field $\boldsymbol{B}_{\rm AC}$ of angular frequency ω perpendicular to the static field $\boldsymbol{B}_0$. In the rotating frame, the Hamiltonian[36] can be written as

$$H_{\rm ESR} = \frac{\hbar(\omega_z - \omega)}{2}\sigma_z + \frac{\hbar\omega_1}{2}[\sigma_x \cos\phi - \sigma_y \sin\phi], \quad (4)$$

where we assume $\boldsymbol{B}_{\rm AC} = \boldsymbol{x}\boldsymbol{B}_{\rm AC}\cos(\omega t + \phi)$ and define $\omega_1 \equiv g\mu_{\rm B}\boldsymbol{B}_{\rm AC}/2$. If the oscillating magnetic field frequency $f_{\rm AC} = \omega/2\pi$ matches the Larmor frequency, namely on resonance, the first term in the Hamiltonian will vanish, leading to a reduced Hamiltonian:

$$H_{\rm ESR} = \frac{\hbar\omega_1}{2}[\sigma_x \cos\phi - \sigma_y \sin\phi]. \quad (5)$$

Spin will rotate around the x axis with a frequency of $f_{\rm Rabi} = \omega_1/2\pi$ when ϕ equals zero, which is called Rabi oscillation. Furthermore, we can use a sequence of magnetic field pulses with different durations to control the amount of rotation and different phases to select the rotation axis to achieve full control. The universal single spin qubit control has been realized in Si MOS quantum dot by Veldhorst *et al*. in 2014. As shown in Fig. 5(a), they implement ESR by introducing a transmission line adjacent to their quantum dot, showing gate fidelity as high as 99.6%, which was measured using a randomized benchmarking method[37] as shown in Fig. 5(b).

However, the manipulation rate of the ESR technique is relatively low (< 1 MHz) because a strong oscillating magnetic field is hard to produce on chip. In comparison, an electric field is more convenient to apply on chip and to benefit from it, different EDSR techniques have been extensively studied. The EDSR technique utilizes electric fields instead of magnetic fields to manipulate electron spins and therefore, a mediating mechanism that couples the electric field to spin should be brought in. Usually, the mediating mechanism is an inhomogeneous magnetic field from an integrated micro-magnet[38] or spin–orbit coupling[39] of the material. In this way, the oscillating electric field drives the electron periodically displaced in the inhomogeneous magnetic field, thus the electron feels an effective oscillating magnetic field like in ESR. In silicon, spin–orbit coupling is supposed to be so small and an integrated micro-magnet are more frequently used. Using the micro-magnet method, the manipulation rate can be as high as 30 MHz by Tarucha's group in 2017 based on an Si/SiGe quantum dot with gate fidelity exceeding 99.9%, which strongly underpins the prospects for universal quantum computing.[40]

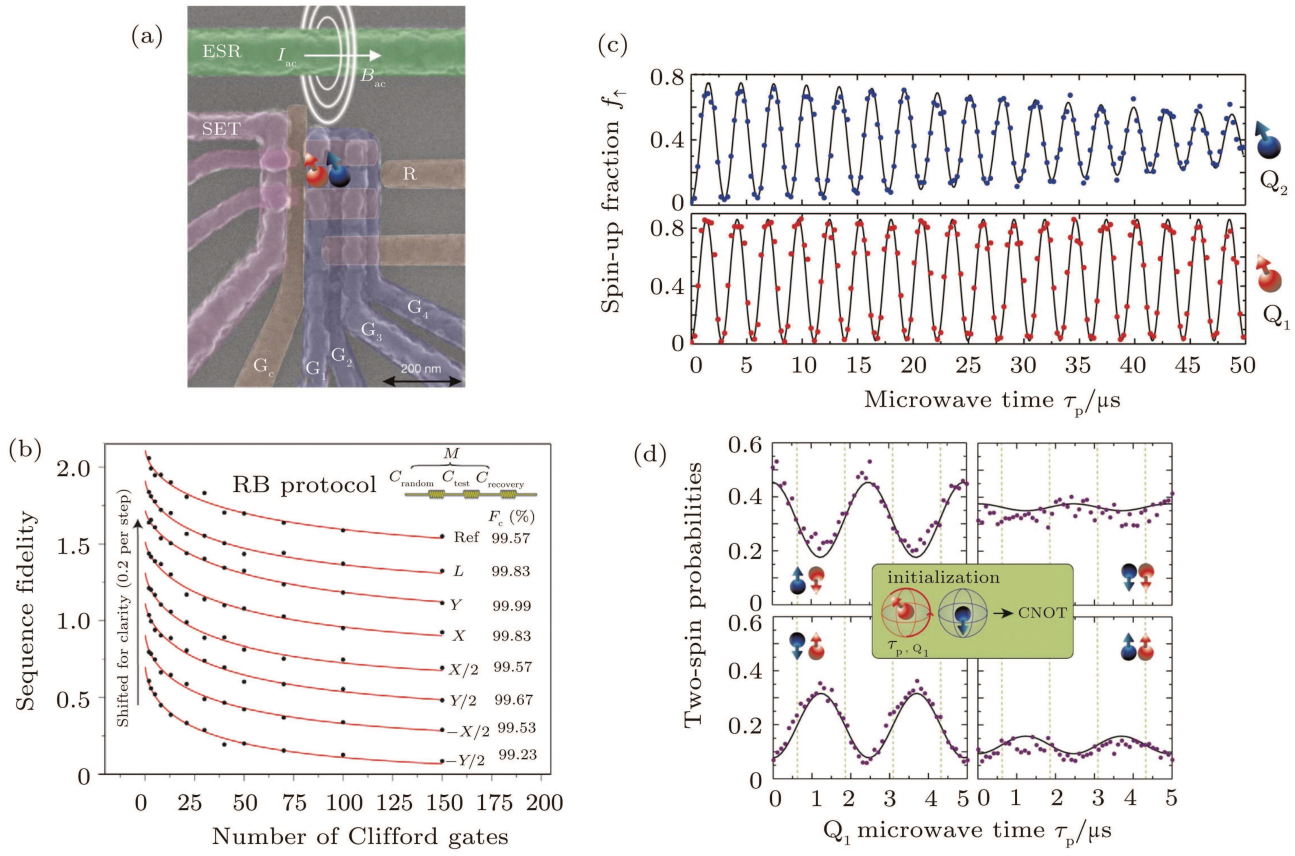


Fig. 5. (color online) Experimental demonstration of spin qubits. (a) SEM image of the silicon CMOS quantum dot for single- and two-qubit operations. The spin states of two qubits are controlled by the magnetic field $B_{\rm AC}$ produced by the ESR transmission line with ac current $I_{\rm ac}$. A single or double quantum dot can be formed by adjusting the voltages of gates G_1–G_4. G_c denotes the confinement gate while R denotes the reservoir.[5] (b) Fidelity of a single qubit formed in the device of panel (a) through randomized benchmarking of Clifford gates. From the decay an average fidelity of 99.6% can be inferred.[37] (c) Rabi oscillations of individual spin qubit in each quantum dot of panel (a).[5] (d) Two-spin probabilities as functions of the microwave pulse length $\tau_{\rm p}$ on the control qubit (Q_1) after applying a CNOT gate (the inset shows the corresponding Bloch sphere). Black solid lines are the fits based on a CNOT gate considering read-out errors while green dotted lines show the intended maximally entangled states.[5]

The readout of the spin state is realized by spin–charge conversion.[41] As illustrated in Figs. 6(a) and 6(b), this conversion can either rely on the energy or the tunnel rate difference of two opposite spin states. For the first method, it requires the Fermi level of the drain to be between the state $|0\rangle$ and $|1\rangle$, and the state with energy higher than the Fermi level can tunnel from the dot to the drain while the opposite state is a blockade. In the second method, both states can tunnel out of the dots but the tunnel rate depends strongly on the spin state. If the measurement time is put in between these two tunnel rates, one can tell the spin state by observing whether the tunneling happens or not.

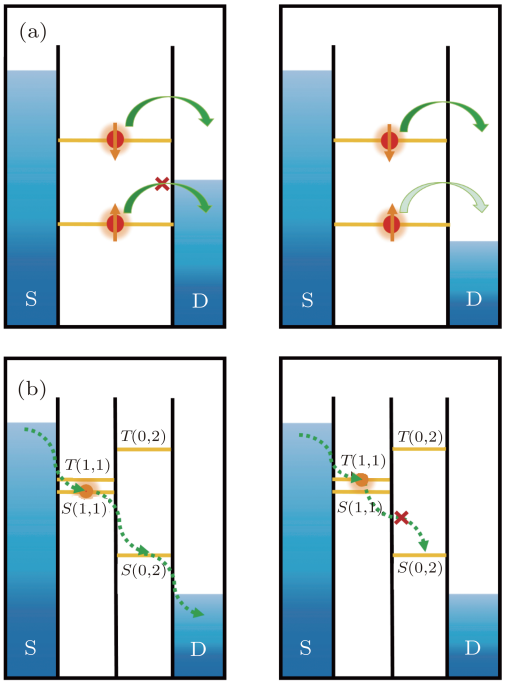


Fig. 6. (color online) Energy diagrams explaining spin–charge conversion and Pauli spin blockade for qubit readout. (a) Energy-selective readout (left) and tunnel-rate-selective readout (right) are shown. The electron of the spin-up state in the energy-selective readout regime is not allowed to tunnel out of the dot since its energy level is below the Fermi energy level of drain (D) while its tunnel rate is much slower in the tunnel-rate-selective readout regime (denoted by the translucent arrow) and cannot be detected by the charge sensor during the measurement. (b) $S(1,1)$ can be converted to $S(0,2)$ (left) while $T(1,1)$ cannot (right), thus a current through source (S) and drain (D) can be detected only if the qubit is in the singlet state and thus these two states can be distinguished. Or a charge sensor that can tell $(0,2)$ from $(1,1)$ is also able to read the spin state.

Following the original proposal, a two qubit gate based on spin qubits can be implemented through an exchange interaction allowed by the tunnel coupling between two quantum dots. The Hamiltonian[36] can be described as

$$H_{\rm TS} = J\boldsymbol{S}_1 \cdot \boldsymbol{S}_2 + g\mu_{\rm B}\boldsymbol{B}_0 \cdot (\boldsymbol{S}_1 + \boldsymbol{S}_2), \tag{6}$$

where $\boldsymbol{S}_\nu$ ($\nu = 1/2$) represents a localized electron spin in the dots 1 and 2, and J represents their exchange coupling. The estimation of J is vital to the two spin qubit operation. Through the control of J between the qubits via the detuning energy ε, one can realize a chosen two qubit gate. In 2015, researchers from Australia first demonstrated a CNOT gate via controlled-phase operations combined with single-qubit operations based on Si CMOS quantum dots.[5] Rabi oscillations of individual qubit and the anticorrelations between antiparallel spin states after a CNOT operation that characterize the two qubit gate are illustrated in Figs. 5(c) and 5(d), respectively. Later in 2017, Petta *et al*. showed a 200-ns CNOT gate directly by turning on an exchange interaction,[42] nearly an order of magnitude faster than the previous one, and created a Bell state with a fidelity $F = 75\%$. In the meanwhile, Vandersypen *et al*. performed Deutsch–Josza and the Grover search algorithms based on Si/SiGe quantum dots,[43] and their Bell states showed fidelities between 85%–89%. Although the fidelity of the two qubit gate is still challenging to surpass the threshold value of fault tolerant quantum computing, these results have paved the way for a large scale quantum computer.

Moreover, spin exists not only in electrons but also holes in semiconductors. A number of extensive researches have been performed on holes in quantum dots based on Si MOS,[44,45] GaAs/AlGaAs heterostructure,[46] and semiconductor nanowires.[47,48] Recently, Maurand *et al*. reported a hole spin qubit based on an industry-standard fabricated CMOS quantum dot via EDSR, in which the Rabi frequency reached 85 MHz, much larger than that in electrons.[49] However, the decoherence time is relatively short, about only 59 ± 1 ns, the origin of which is still unknown and further study will be necessary to realize a high fidelity hole spin qubit.

3.3. Singlet-triplet qubit

Utilizing the exchange interaction between two spins, Petta *et al*. also proposed an 'effectively single qubit' called singlet-triplet (ST) qubit.[10] The energy spectrum of the ST qubit as a function of detuning is shown in Fig. 3, which is operated in the vicinity of the $(1,1)$–$(0,2)$ charge transition of a double quantum dot. The ground state $|0\rangle$ and excited state $|1\rangle$ are encoded by the singlet states $S(1,1) = (|\uparrow\downarrow\rangle - |\downarrow\uparrow\rangle)/\sqrt{2}$ and $T_0(1,1) = (|\uparrow\downarrow\rangle + |\downarrow\uparrow\rangle)/\sqrt{2}$. For sufficiently negative detunings, $S(1,1)$ and $T_0(1,1)$ are nearly degenerate. A magnetic field $\boldsymbol{B}_0$ splits off $T_+(1,1) = |\uparrow\uparrow\rangle$ and $T_-(1,1) = |\downarrow\downarrow\rangle$ by the Zeeman energy. Near $\varepsilon = 0$, the singlet states $S(1,1)$ and $S(0,2)$ are hybridized due to the interdot tunnel coupling $2t$, which causes an energy splitting $J(\varepsilon)$ between $T_0(1,1)$ and $S(1,1)$, forming a qubit with an effective Hamiltonian[18]

$$H_{\rm ST} = -\frac{J(\varepsilon)}{2}\sigma_z + g\mu_{\rm B}\Delta B_{N,z}\sigma_x, \tag{7}$$

where $\Delta B_{N,z}$ refers to the difference in random hyperfine fields along the applied field direction. If $J(\varepsilon)$ is much greater than

$g\mu_B\Delta B_{N,z}$, which can be accomplished by adjusting the detuning ε in experiments, the qubit will rotate around the z axis. To rotate it around the x axis, a strong, stable difference in Zeeman splitting between two quantum dots is needed instead of the second term in the Hamiltonian that is weak and unstable. Usually, this is achieved by dynamic nuclear polarization[50] or integrating a micro-magnet.[51] Applying the former method in GaAs quantum dots, Yacoby's group measured single-qubit gate fidelities of ~99%,[52] which is illustrated in Fig. 7(b).

The readout of the ST qubit is achieved by the so-called Pauli spin blockade.[53] As figure 6(b) shows, the singlet state $S(1,1)$ can adiabatically follow to $S(0,2)$ while the triplet state $T_0(1,1)$ remains in a spin blockade $(1,1)$ charge state. Hence a charge sensing signal of $(0,2)$ indicates the qubit remains in the $|0\rangle$ and a signal of $(1,1)$ indicates that the qubit rotates into $|1\rangle$. A readout in the singlet-triplet basis usually has higher fidelity than the traditional spin–charge conversion, and recent progress suggests its potential for a higher fidelity spin readout.[54–57]

Two qubit gates based on the ST qubit can be realized by two adjacent ST qubits that are capacitively coupled. In this way, different states in the first qubit will impose different electric fields on the other due to the Pauli exclusion principle, and this difference causes a shift in the precession frequency of the second qubit, leading it to rotate conditionally. In 2012, Yacoby's group first demonstrated the entanglement of ST qubits in this way and their device is shown in Fig. 7(a). Later, they suppressed charge noises by applying large transverse qubit energy splitting that are not sensitive to charge fluctuations, yielding an entangling gate fidelity of 90% via process tomography,[52] which are illustrated in Figs. 7(c) and 7(d). Considering its high manipulation rate and simple control technique gained by electrical operation, as well as the relatively high fidelity realized recently, the ST qubit deserves more research to be isotopically enhanced for quantum computing.[54]

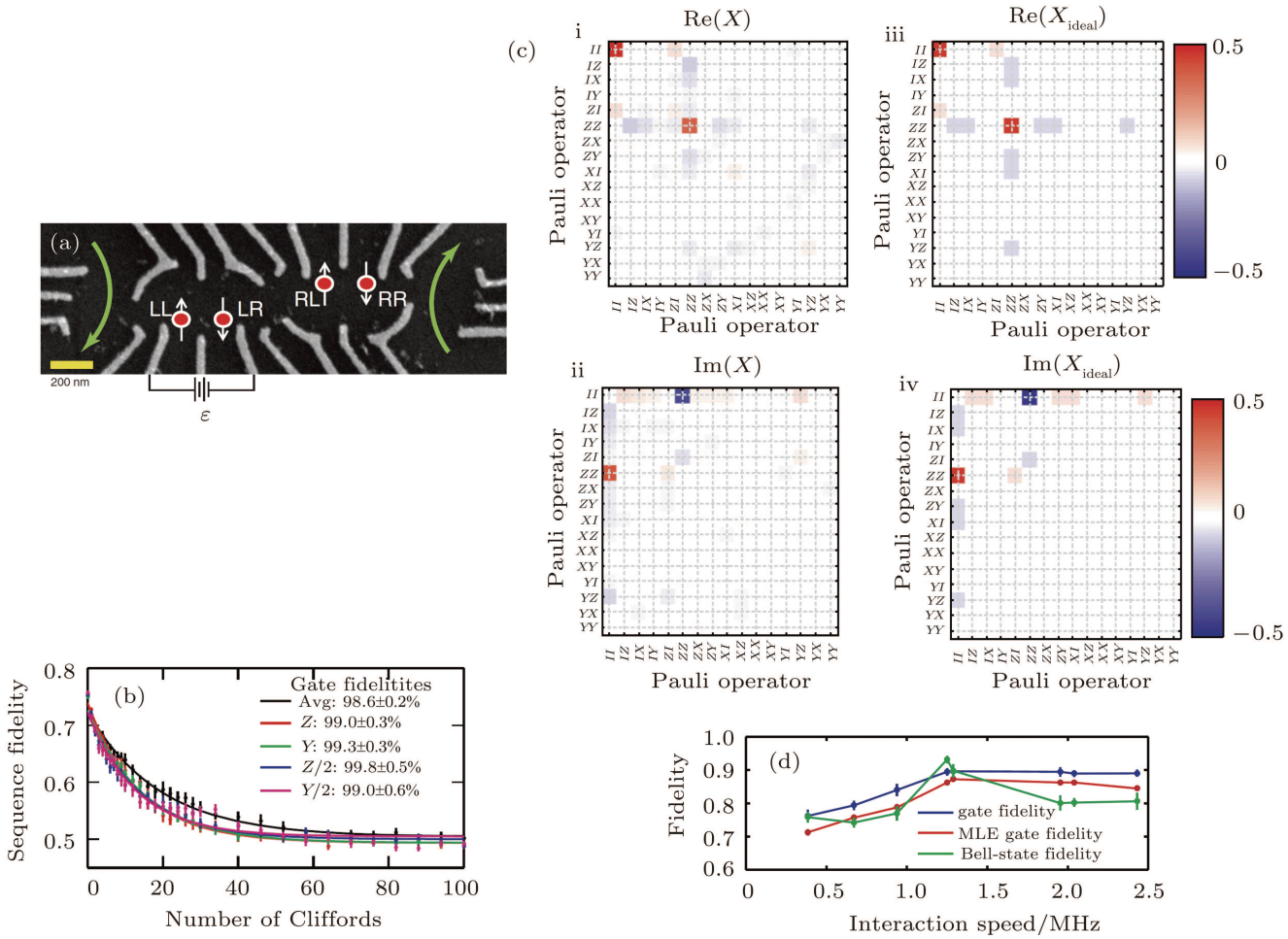


Fig. 7. (color online) Experimental demonstration of ST qubits:[52] (a) SEM image of a device for two ST qubit gate. The green arrows denote current paths for charge sensing and electrons in the left qubit is labeled LL and LR while electrons in the right qubit is labeled RL and RR. (b) Fidelity of a single qubit formed in the device of panel (a) through randomized benchmarking. From the decay an average fidelity of 98.6% can be inferred. (c) Process tomography for the two-qubit entangling gate. i and ii are real and imaginary components of the measured process matrix, respectively, while iii and iv are of the ideal process matrix. (d) Gate fidelity of the measured process matrix and most-likely completely positive process matrix (attained by maximum likelihood estimation process) and two-qubit Bell state fidelity as a function of the interaction strength between two ST qubits, yielding maximum fidelity of 90±1%, 87±%, and 93±1%, respectively. Error bars are statistical uncertainties.

3.4. Exchange qubit

Though ST qubit can be manipulated electrically, a stable magnetic field gradient is still needed for universal control. Another method to establish a qubit in quantum dots is to use solely the exchange interaction, in which way the universal control can be realized fully electrically. Such qubit is called the exchange qubit that is made up of three spins in a triple quantum dot, and the coherent spin manipulation is within a two-spin subspace. Exchange qubits can be divided into two categories : exchange-only qubits[58] and resonant exchange qubits.[59]

3.4.1. Exchange-only qubit

A triple quantum dot is shown in Fig. 8(a), and we denote $(N_{\rm l}, N_{\rm m}, N_{\rm r})$ for the electron arrangement. Three-electron-spin states are more complicated than two spins, but we restrict ourselves only to the subspace $(1,1,1)$, $(2,0,1)$, and $(1,0,2)$. The energy spectrum is characterized in Fig. 3, where we suppose left and right inter-dot tunnel couplings are equal,

$$|0\rangle = \frac{1}{\sqrt{6}}(|\uparrow\uparrow\downarrow\rangle + |\downarrow\uparrow\uparrow\rangle - 2|\uparrow\downarrow\uparrow\rangle),$$
$$|1\rangle = \frac{1}{\sqrt{2}}(|\uparrow\uparrow\downarrow\rangle - |\downarrow\uparrow\uparrow\rangle)$$

are eigenstates in the center of $(1,1,1)$. The ground state $|0\rangle$ connects continuously to a singlet state of the left pair, $|S_{\rm l}\rangle = (1/\sqrt{2})(|\uparrow\downarrow\uparrow\rangle - |\downarrow\uparrow\uparrow\rangle)$ in $(2,0,1)$ and to one of the right pair, $|S_{\rm r}\rangle = (1/\sqrt{2})(|\uparrow\uparrow\downarrow\rangle - |\uparrow\downarrow\uparrow\rangle)$ in charge state $(1,0,2)$. So the ground state $|0\rangle$ can tunnel into (2,0,1) or (1,0,2) for readout while the excited state $|1\rangle$ is a triplet state that cannot tunnel into those states due to spin blockade and thus the qubit state can be characterized. There are still two other states left: $|Q_+\rangle = |\uparrow\uparrow\uparrow\rangle$ intersecting $|0\rangle$ at two anticrossings and

$$|Q\rangle = \frac{1}{\sqrt{3}}(|\uparrow\uparrow\downarrow\rangle + |\uparrow\downarrow\uparrow\rangle + |\downarrow\uparrow\uparrow\rangle)$$

separated from the excited state $|1\rangle$ by a sizable gap. The effective Hamiltonian[60] can be written as

$$H_{\rm EO} = J_{\rm l}(\varepsilon)\sigma_{\rm l} + J_{\rm r}(\varepsilon)\sigma_{\rm r}, \tag{8}$$

where $\sigma_{\rm l} \equiv (\sqrt{3}\sigma_x - \sigma_z)/4$, $\sigma_{\rm r} \equiv (-\sqrt{3}\sigma_x - \sigma_z)/4$, and $J_{\rm l}(\varepsilon)$ and $J_{\rm r}(\varepsilon)$ are exchange interactions between the left dot and the middle dot, and the middle dot and the right dot, respectively. As illustrated in Fig. 8(b), $J_{\rm l}(\varepsilon)$ and $J_{\rm r}(\varepsilon)$ drive rotations about axes that are 120° apart on the Bloch sphere. This two-axis control can in principle be utilized to accomplish arbitrary control of the qubit.

The universal control of an exchange-only qubit has been realized both in GaAs[58,60] and Si/SiGe quantum dots.[61] However, they both suffer severely from the charge noise. Recently, a method called symmetric operation[62,63] which reduces the effect of the charge noise by a factor of 5 or 6 is proposed. Further research in three quantum dots is required to prove its feasibility.

3.4.2. Resonant exchange qubit

The resonant exchange qubit is a modified version of an exchange-only qubit which is operated through resonant driving of the qubit energy gap induced by the always turned on exchange interaction. Further, due to the advantage of resonant driving, the operating point is within a narrowband response only to high frequency electrical noise, which protects the qubit against low-frequency electrical noise. Compared to the exchange-only qubit, the energy spectrum remains unchanged, only the gap between qubit states and $|Q\rangle$ is deliberately kept large by setting $J_{\rm l}$ and $J_{\rm r}$ to be large throughout the $(1,1,1)$. The effective Hamiltonian[64] can be rewritten as the following expression

$$H_{\rm RX} = -\frac{1}{2}J_z\sigma_z - \frac{1}{2}J_x\sigma_x, \tag{9}$$

where $J_z = (1/2)[J_{\rm l}(\varepsilon) + J_{\rm r}(\varepsilon)]$ and $J_x = (\sqrt{3}/2)[J_{\rm r}(\varepsilon) - J_{\rm l}(\varepsilon)]$. Qubit rotations can be controlled by applying an oscillating voltage to a certain gate, like $V_{\rm l}$ in Fig. 8(b), which moves the operating point around $\varepsilon = 0$, providing an oscillatory transverse field J_x. When the oscillation frequency ω matches the exchange frequency, $J_z/\hbar$, the qubit oscillates between the ground state and the excited state. This can be understood more concretely by the Hamiltonian on resonance in the rotating frame:

$$H_{\rm Rot} = \cos(\phi)\sigma_x + \sin(\phi)\sigma_y, \tag{10}$$

which is similar to the Hamiltonian used in the ESR control of a spin qubit and ϕ is the relative phase of the carrier wave with respect to the first pulse incident on the qubit. Phase controlling relative to the initial pulse thus allows a full qubit control.

The experimental demonstration of resonant exchange qubits was realized by Marcus's group[64] in 2013. As illustrated in Fig. 8(c), they extended the decoherence time T_2^* by applying Carr–Purcell–Meiboom–Gill (CPMG)-n pulses, showing coherence time T_2 up to 19±2 μs, which is much higher than an exchange-only qubit. Until now, however, the two qubit gate by exchange-only qubit or resonant exchange qubit has not been demonstrated in experiments. Nevertheless, the large dipole moment of three-spin qubits makes it promising for fast long-ranged two-qubit interactions utilizing a cavity as a mediator.[65] Recently, Landig *et al*. demonstrated the strong coupling between the three-spin qubit and the cavity photons,[66] which is an essential step towards the two-qubit interactions.

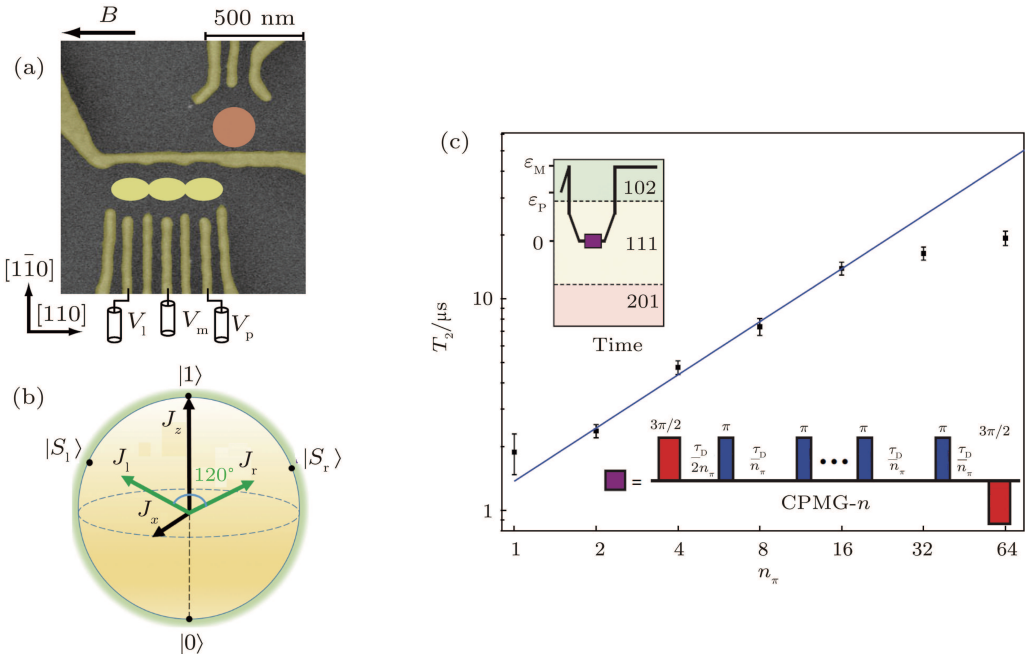


Fig. 8. (color online) Experimental demonstration of exchange qubits. (a) False-color SEM image of a device fabricated for both the exchange-only qubit and the resonant exchange qubit.[60] Triple quantum dots are denoted by small red circles while a bigger quantum dot acting as a charge sensor like a QPC channel is denoted by a big red circle. Voltages applied on V_l and V_r are used to control the charge occupancy of the left and right dots as well as the detuning ε. (b) Schematic diagram of the effects of J_l, J_r on the exchange-only qubit, J_x and J_z on the resonant exchange qubit via Bloch sphere. Two initialization states, $|S_l\rangle$ and $|S_r\rangle$ are also included. (c) Coherence time T_2 of a resonant exchange qubit[64] for various orders of CPMG-n pulses. The lower inset demonstrates that each CPMG dynamical decoupling sequence includes $n\pi$ rotations around the y axis while the upper inset shows the detuning sequence in the energy level spectrum. The fit denoted by the blue line suggests the coherence time is up to 19±2 μs.

3.5. Hybrid qubit

Though the exchange qubit can be realized by full electrical control, two detunings, ε_l and ε_r are required for adjusting J_l and J_r, which are hard to optimize in experiments. Another idea of how to implement all electric control is the hybrid qubit, which is based on the spin states of three electrons in a double quantum dot.[12,67,68] The ground state and the excited state are $|0\rangle \equiv |S\rangle_L|\downarrow\rangle_R$ and

$$|1\rangle \equiv -\sqrt{\frac{2}{3}}|T_-\rangle_L|\uparrow\rangle_R + \frac{1}{\sqrt{3}}|T_0\rangle_L|\downarrow\rangle_R,$$

respectively, where the left quantum dot is occupied doubly while the right quantum dot only singly. The energies of $|0\rangle$ and $|1\rangle$ versus detuning ε between the two dots are depicted in Fig. 3, transitions between $|0\rangle$ and $|1\rangle$ can be performed by first putting the qubit near the avoided crossing between $|0\rangle$ and $|E\rangle$ at detuning ε_A and then drive it towards the anticrossing between $|1\rangle$ and $|E\rangle$ at ε_B. As illustrated in Fig. 9(a), the excited state $|E\rangle = |\downarrow\rangle_L|S\rangle_R$ here is used for mediation. In addition, a phase between $|0\rangle$ and $|E\rangle$ can accumulate when the qubit is at detuning ε_P, leading to a rotation around the z axis. In combination with the rotation around the x axis caused by oscillations between $|0\rangle$ and $|1\rangle$, a pulse sequence $\varepsilon_i \to \varepsilon_B \to \varepsilon_P \to \varepsilon_A \to \varepsilon_P \to \varepsilon_B \to \varepsilon_f$ can implement rotations about any axis of the Bloch sphere.[69] In this way, the detuning ε is the only control parameter, which is much simpler for operations in contrast to the exchange qubit.

Also, from the perspective of the Hamiltonian,[70] the hybrid qubit can be described as

$$H_H = \hbar\omega_z\sigma_z + j\sigma_x, \tag{11}$$

where $\hbar\omega_z \simeq E_{ST}$, meaning the energy gap between the qubit state is dominated by the orbital singlet-triplet splitting E_{ST}, which can be controlled solely by gate voltages. The x rotation can be realized by adjusting $j \propto J_S + J_T$ with proportionalities $J_{S,(T)} \propto (2t_{S,(T)})^2/\Delta E_{S,(T)}$, where $J_{S,(T)}$, $2t_{S,(T)}$ and $\Delta E_{S,(T)}$ are the corresponding exchange coupling strength, tunneling amplitude and energy difference between the state $|E\rangle$ and the singlet (triplet) state. Therefore, considering all the parameters here can be controlled electrically, the two-axis control of the hybrid qubit removes the need for a magnetic field gradient in contrast to ST qubits.

In experiments, fidelities of 93% for x rotations and 96% for z rotations have been yielded in Si/SiGe quantum dots by Dohun Kim *et al.* in 2015.[71] Recently, hybrid qubits were also implemented in GaAs quantum dots that are encoded at the (2,3)–(1,4) charge transition,[54] yielding a decoherence time of $T_2^* = 8.10$ ns and a Larmor frequency of almost 2.5 GHz. This combination of relative long decoherence time and high speed manipulation proves its superiority over traditional charge or spin qubits. The device image and the Larmor oscillations for the measurement of T_2^* and Larmor frequency are shown in Figs. 9(b) and 9(c).

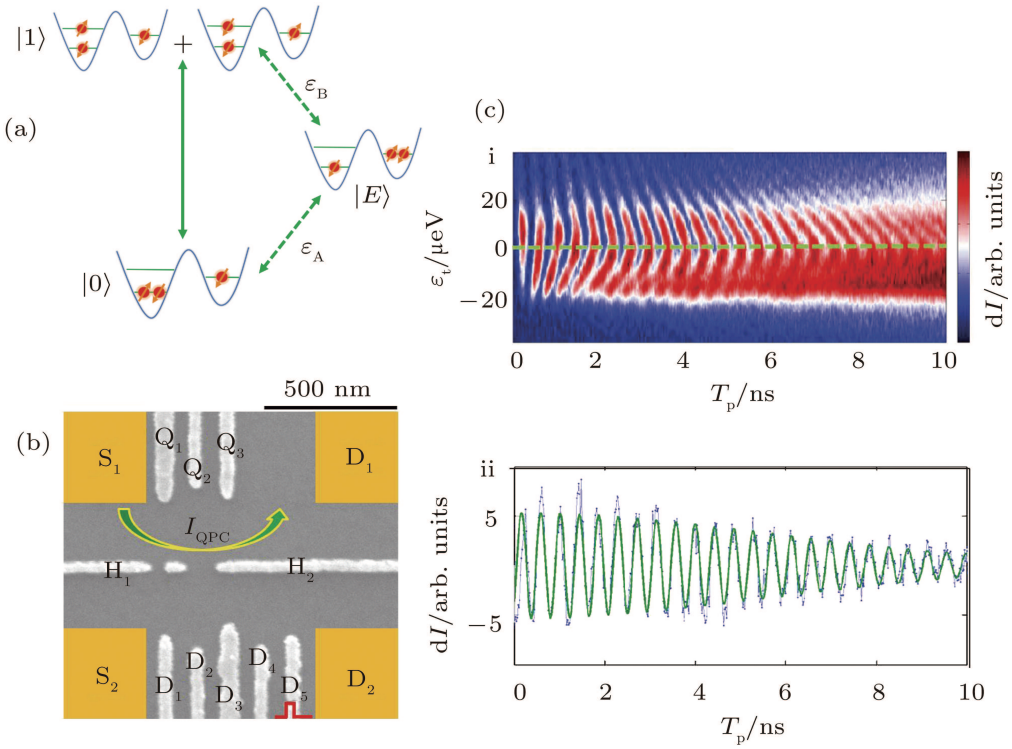


Fig. 9. (color online) Experimental demonstration of hybrid qubits. (a) Schematic diagram of the physics underlying transitions between $|0\rangle$ and $|1\rangle$. Dashed green arrows connect $|0\rangle$ and $|1\rangle$ with $|E\rangle$, and the effective transition between the two basis states is indicated by the solid green arrow. ε_A and ε_B mark the detunings where transitions happen. (b) SEM image of a device fabricated for hybrid qubits.[72] I_{QPC} is denoted by a red arrow while S1, S2 and D1, D2 denote source and drain. (c) The Larmor precession of the hybrid qubit working at the $(2,3)$–$(1,4)$ charge transition.[72] Charge oscillations are depicted in i as a function of the nonadiabatic pulse width T_p and ε_t (ε_t is defined as the energy detuning relative to the anticrossing point between the qubit levels), while ii shows the signal along the green dashed lines plotted in i. The green solid line in ii is a numeral fit and from which a dephasing time of $T_2^* = 8.10$ ns can be extracted.

4. Long range coupling of qubits

To realize a large-scale universal quantum computer, it is believed that quantum error correction (QEC) is indispensable, which is a technique that builds logical qubits upon physical qubits to avoid realistic faults during qubit operations, provided that the errors are below a fault-tolerant threshold.[73] Among the different approaches for QEC, the surface code[74] is most promising, which requires a two-dimensional geometry of qubits. However, for quantum dot based qubits, the multiple electrodes limit the possibility to connect one qubit with four qubits around. To overcome this technical difficulty, long range coupling like cavity quantum electrodynamics (cQED) is introduced.[75]

The interaction between light confined in a cavity and atoms is called the cavity quantum electrodynamics. By using such interaction, the spin states and charge states of distant electrons can be coupled together. To implement this interaction for quantum dot based qubits, the strong coupling between electrons and photons should be first demonstrated. However, for a very long time the interaction between electrons in the quantum dots and microwave photons cannot step into the strong coupling regime, although it has been realized based on different quantum dots varying from GaAs/AlGaAs heterostructure,[76] semiconductor nanowires,[77] carbon nanotubes,[75] to even graphene.[78–80] In the strong coupling regime, the coherent coupling rate between the two-level atom and the cavity photon g_c must exceed the photon loss rate κ and the atomic decoherence rate γ. Last year, three groups achieved this goal using GaAs/AlGaAs,[81,82] Si/SiGe,[83,84] and carbon nanotube[85] based quantum dots at nearly the same time. The device for the coupling between Si/SiGe quantum dots and superconducting cavity is shown in Figs. 10(a)–10(c), and the clear vacuum Rabi splitting shown in Figs. 10(d) and 10(e) indicates the realization of strong coupling. These results strengthen the faith for coupling distant qubits and opens a new way for quantum dot based quantum computing.

Another consideration for coupling two distant qubits is the spin degree of electrons. Spin is much more isolated from its environment than the electronic charge, leading to an extremely weak coupling to the electromagnetic field of a cavity with the effective coupling strength $g_{spin} \simeq 50$ Hz.[86] To increase the coupling strength, one way is to utilize the large charge–photon coupling to create an effective spin electric dipole moment. This method requires a magnetic field gradient, and the origin of the magnetic field gradient can be spin–

orbit coupling,[77] an integrated ferromagnetic reservoir[87] or a micromagnet.[88,89] Recently, Mi *et al.*[88] and Samkharadze *et al.*[89] both demonstrated strong spin–photon coupling with a coupling rate higher than 10 MHz in silicon, and Mi *et al.* also used cavity photons to show the dispersive readout of a single spin after coherent control. These results shed light on entangling spin qubits using photons.

Except for the cQED method, long range coupling can also be achieved by surface acoustic waves,[90,91] superexchange interaction[92] or through a solid state flying qubit.[93] These methods together make a promise for the future use in a realistic quantum computer.

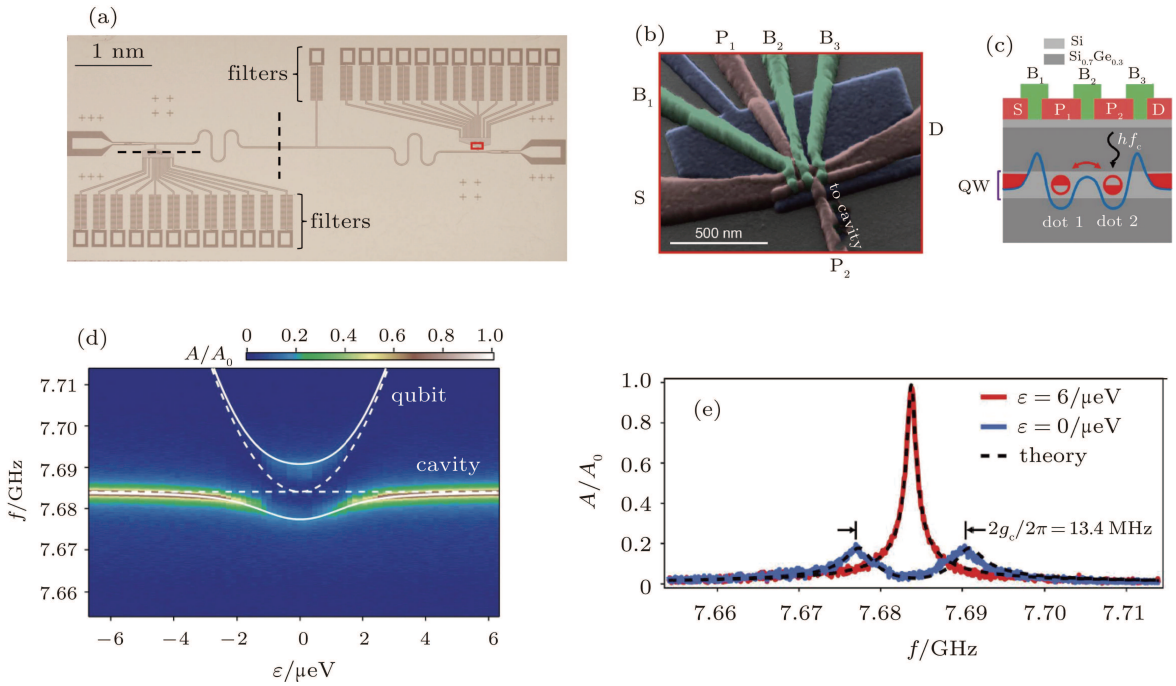


Fig. 10. (color online) Experimental demonstration of the hybrid circuit quantum electrodynamics.[83,84] (a) Optical image of a silicon hybrid circuit quantum electrodynamics device that was used to demonstrate strong coupling. An Si double quantum dot indicated by the red box is placed at the voltage anti-node of the cavity. LC filters are used to improve cavity quality. (b) False color SEM image of the Si quantum dot used in panel (a). Gate P2 is used to connect the cavity while playing the role of a plunger gate in the double quantum dot. (c) Schematic cross section of the double quantum dot. An excess electron is confined in the quantum well (QW) denoted by the blue line, while a cavity photon with energy hf_c interacting with the electron is denoted by a black arrow, where h is the Planck's constant and f_c is the photon frequency. (d) Cavity transmission spectrum A/A_0 as a function of photon frequency f and detuning ε with $2t/h = f_c = 7.68$ GHz, where t is the interdot tunnel coupling. Solid lines are system eigenenergies at the case of $g_c/2\pi = 6.7$ MHz while dashed lines are those of no coupling. (e) A/A_0 as a function of f at $\varepsilon = 6$ μeV and 0 μeV. Dashed lines are theoretical predictions. The normal mode splitting shown by two blue peaks indicates the strong coupling regime is reached.

5. Conclusion and perspectives

Since DiVincenzo first proposed qubits based on quantum dots in 1998,[11] different types of qubits utilizing different degrees of electrons or holes in diverse materials develop fast during the last 20 years. There are also some other hybrid types of qubits[94–97] that are not included in this paper owing to space reasons, but the qubits discussed here are enough for us to talk about the future trends of qubits based on quantum dots. Until now, it is still so hard to tell which type is better or has greater potential for future development. However, we can compare two different characteristics that are considered most for qubit implementations: fidelity and scalability.

From the view of fidelity, spins in silicon driven by ESR or EDSR are most promising. Recent advances in Si MOS quantum dots and undoped Si/SiGe quantum dots proved high fidelity single and two qubit gates, and prototype quantum algorithms based on two qubits were even demonstrated.[5,42,43] Further developments will concentrate on two qubit gates with fidelity at the surface code threshold for fault tolerance, and QEC of multiple qubits, of which one proposal has been presented based on Si MOS qubits.[98] However, due to the inhomogeneity and variability introduced by the integrated components and complicated electrode arrangement, the scalability of spin qubits is questionable. Simpler manipulations and readout are worth further research. Recent reports on utilizing spin–orbit coupling at the MOS interface to implement ESR[55,99] and using gate sensors for readout[100–104] offer new opportunities.

On the other hand, if we consider more on scalability, qubits that can be manipulated all electrically are more promising. From this point of view, charge qubits, exchange qubits and hybrid qubits are better. Nevertheless, these qubits suffer more from charge noises and the fidelities of them are limited. Recent improvements like symmetric operation[62,63] and large detuning working point[105] seems a good way to solve this problem. Further progress must reside in the im-

provement of fidelity, which in turn will decide which type is better.

To draw a conclusion, fidelity and scalability both play significant roles in the development of quantum computing. Whatever the future qubit type is, requirements must be met from both sides. The good news is, qubits based on semiconductor quantum dots now are close to these requirements and several different architectures of the quantum dot-based quantum computer have been promoted recently.[106–109] More or less, qubits based on semiconductor quantum dots are now on the way to build a fault-tolerant quantum computer in the near future.

References

[1] You J Q and Nori F 2011 *Nature* **474** 589
[2] Gu X, Kockum A F, Miranowicz A, Liu Y X and Nori F 2017 arXiv: 1707.02046v2 [quant-ph]
[3] Monroe C and Kim J 2013 *Science* **339** 1164
[4] Pla J J, Tan K Y, Dehollain J P, Lim W H, Morton J J L, Jamieson D N, Dzurak A S and Morello A 2012 *Nature* **489** 541
[5] Veldhorst M, Yang C H, Hwang J C, Huang W, Dehollain J P, Muhonen J T, Simmons S, Laucht A, Hudson F E, Itoh K M, Morello A and Dzurak A S 2015 *Nature* **526** 410
[6] Li H O, Yao B, Tu T and Guo G P 2012 *Sci. Bull.* **57** 1919
[7] Hayashi T, Fujisawa T, Cheong H D, Jeong Y H and Hirayama Y 2003 *Phys. Rev. Lett.* **91** 226804
[8] Loss D and DiVincenzo D P 1998 *Phys. Rev. A* **57** 120
[9] Kolodrubetz M H and Petta J R 2009 *Science* **325** 42
[10] Petta J R, Johnson A C, Taylor J M, Laird E A, Yacoby A, Lukin M D, Marcus C M, Hanson M P and Gossard A C 2005 *Science* **309** 2180
[11] DiVincenzo D P, Bacon D, Kempe J, Burkard G and Whaley K B 2000 *Nature* **408** 339
[12] Kim D, Shi Z, Simmons C B, Ward D R, Prance J R, Koh T S, Gamble J K, Savage D E, Lagally M G, Friesen M, Coppersmith S N and Eriksson M A 2014 *Nature* **511** 70
[13] Hanson R, Kouwenhoven L P, Petta J R, Tarucha S and Vandersypen L M K 2007 *Rev. Mod. Phys.* **79** 1217
[14] Koppens F H, Buizert C, Tielrooij K J, Vink I T, Nowack K C, Meunier T, Kouwenhoven L P and Vandersypen L M K 2006 *Nature* **422** 766
[15] Nowack K C, Shafiei M, Laforest M, Prawiroatmodjo G E, Schreiber L R, Reichl C, Wegscheider W and Vandersypen L M K 2011 *Science* **02** 1269
[16] Tyryshkin A M, Tojo S, Morton J J, Riemann H, Abrosimov N V, Becker P, Pohl H J, Schenkel T, Thewalt M L, Itoh K M and Lyon S A 2012 *Nat. Mater.* **11** 143
[17] Shaji N, Simmons C B, Thalakulam M, Klein L J, Qin H, Luo H, Savage D E, Lagally M G, Rimberg A J, Joynt R, Friesen M, Blick R H, Coppersmith S N and Eriksson M A 2008 *Nat. Phys.* **4** 540
[18] Maune B M, Borselli M G, Huang B, Ladd T D, Deelman P W, Holabird K S, Kiselev A A, Alvarado-Rodriguez I, Ross R S, Schmitz A E, Sokolich M, Watson C A, Gyure M F and Hunter A T 2012 *Nature* **481** 344
[19] Li H O, Cao G, Xiao M, You J, Wei D, Tu T, Guo G C, Jiang H W and Guo G P 2014 *J. Appl. Phys.* **116** 174504
[20] You J, Li H O, Cao G, Deng G W, Xiao M and Guo G P 2015 *Europhys. Lett.* **111** 17001
[21] Xiao M, House M G and Jiang H W 2010 *Phys. Rev. Lett.* **104** 096801
[22] Yang C H, Rossi A, Ruskov R, Lai N S, Mohiyaddin F A, Lee S, Tahan C, Klimeck G, Morello A and Dzurak A S 2013 *Nat. Commun.* **4** 2069
[23] Borselli M G, Eng K, Ross R S, Hazard T M, Holabird K S, Huang B, Kiselev A A, Deelman P W, Warren L D, Milosavljevic I, Schmitz A E, Sokolich M, Gyure M F and Hunter A T 2015 *Nanotechnology* **26** 375202
[24] Zajac D M, Hazard T M, Mi X, Wang K and Petta J R 2015 *Appl. Phys. Lett.* **106** 223507
[25] Cao G, Li H O, Tu T, Wang L, Zhou C, Xiao M, Guo G C, Jiang H W and Guo G P 2013 *Nat. Commun.* **4** 1401
[26] Cao G, Li H O, Song X X, Yu G D, Chen B B, Xiao M and Guo G P 2015 *Europhys. Lett.* **112** 37005
[27] Kim D, Ward D R, Simmons C B, Gamble J K, Blume-Kohout R, Nielsen E, Savage D E, Lagally M G, Friesen M, Coppersmith S N and Eriksson M A 2015 *Nat. Nanotechnol.* **10** 243
[28] Fujisawa T, Shinkai G, Hayashi T and Ota T 2011 *Physica E: Low Dimens. Syst. Nanostruct.* **43** 730
[29] Shang R N, Li H O, Cao G, Yu G D, Xiao M, Tu T and Guo G P 2016 *Chin. Phys. Lett.* **31** 050302
[30] Petersson K D, Smith C G, Anderson D, Atkinson P, Jones G A and Ritchie D A 2009 *Phys. Rev. Lett.* **103** 016805
[31] Shinkai G, Hayashi T, Ota T and Fujisawa T 2009 *Phys. Rev. Lett.* **103** 056802
[32] Li H O, Cao G, Yu G D, Xiao M, Guo G C, Jiang H W and Guo G P 2015 *Nat. Commun.* **6** 7681
[33] Li H O, Cao G, Yu G D, Xiao M, Guo G C, Jiang H W and Guo G P 2016 arXiv: 1610.06704v1 [cond-mat]
[34] Ward D R, Kim D, Savage D E, Lagally M G, Foote R H, Friesen M, Coppersmith S N and Eriksson M A 2016 *NPJ Quantum Inf.* **2** 16032
[35] Petta J R, Johnson A C, Taylor J M, Yacoby A, Lukin M D, Marcus C M, Hanson M P and Gossard A C 2006 *Physica E Low Dimens. Syst. Nanostruct.* **34** 42
[36] Tarucha S, Yamamoto M, Oiwa A, Choi B S and Tokura Y 2016 *Principles and Methods of Quantum Information Technologies* (Tokyo: Springer Japan) pp. 541–567
[37] Veldhorst M, Hwang J C, Yang C H, Leenstra A W, de Ronde B, Dehollain J P, Muhonen J T, Hudson F E, Itoh K M, Morello A and Dzurak A S 2014 *Nat. Nanotechnol.* **9** 981
[38] Pioro-Ladriere M, Obata T, Tokura Y, Shin Y S, Kubo T, Yoshida K, Taniyama T and Tarucha S 2008 *Nat. Phys.* **4** 776
[39] Nowack K C, Koppens F H, Nazarov Y V and Vandersypen L M K 2008 *Science* **318** 1430
[40] Yoneda J, Takeda K, Otsuka T, Nakajima T, Delbecq M R, Allison G, Honda T, Kodera T, Oda S, Hoshi Y, Usami N, Itoh K M and Tarucha S 2017 arXiv: 1708.01454v1 [cond-mat]
[41] Hanson R, van Beveren L W, Vink I T, Elzerman J M, Naber W J, Koppens F H, Kouwenhoven L P and Vandersypen L M K 2005 *Phys. Rev. Lett.* **94** 196802
[42] Zajac D M, Sigillito A J, Russ M, Borjans F, Taylor J M, Burkard G and Petta J R 2017 arXiv: 1708.03530v1 [quant-ph]
[43] Watson T F, Philips S G, Kawakami E, Ward D R, Scarlino P, Veldhorst M, Savage D E, Lagally M G, Friesen M, Coppersmith S N, Eriksson M A and Vandersypen L M K 2017 arXiv: 1708.04214v1 [cond-mat]
[44] Li R, Hudson F E, Dzurak A S and Hamilton A R 2015 *Nano Lett.* **15** 7314
[45] Mueller F, Konstantaras G, Spruijtenburg P C, van der Wiel W G and Zwanenburg F A 2015 *Nano Lett.* **15** 5336
[46] Wang D Q, Klochan O, Hung J T, Culcer D, Farrer I, Ritchie D A and Hamilton A R 2016 *Nano Lett.* **16** 7685
[47] Li S X, Li Y, Gao F, Xu G, Li H O, Cao G, Xiao M, Wang T, Zhang J J and Guo G P 2017 *Appl. Phys. Lett.* **110** 133105
[48] Brauns M, Ridderbos J, Li A, Bakkers EP, van der Wiel WG and Zwanenburg F A 2016 *Phys. Rev. B* **94** 041411
[49] Maurand R, Jehl X, Kotekar-Patil D, Corna A, Bohuslavskyi H, Laviéville R, Hutin L, Barraud S, Vinet M, Sanquer M and De Franceschi S 2016 *Nat. Commun.* **7** 13575
[50] Foletti S, Bluhm H, Mahalu D, Umansky V and Yacoby A 2009 *Nat. Phys.* **5** 903
[51] Wu X, Ward D R, Prance J R, Kim D, Gamble J K, Mohr R T, Shi Z, Savage D E, Lagally M G, Friesen M, Coppersmith S N and Eriksson M A 2014 *Proc. Natl. Acad. Sci. USA* **111** 11938
[52] Nichol J M, Orona L A, Harvey S P, Fallahi S, Gardner G C, Manfra M J and Yacoby A 2017 *NPJ Quantum Inf.* **3** 3
[53] Lai N S, Lim W H, Yang C H, Zwanenburg F A, Coish W A, Qassemi F, Morello A and Dzurak A S 2011 *Sci. Rep.* **1** 110
[54] Jock R M, Jacobson N T, Harvey-Collard P, Mounce A M, Srinivasa V, Ward D R, Anderson J, Manginell R, Wendt J R, Rudolph M, Pluym T, Gamble J K, Baczewski A D, Witzel W M and Carroll M S 2017 arXiv: 1707.04357v1 [cond-mat]
[55] Harvey-Collard P, D'Anjou B, Rudolph M, Jacobson NT, Dominguez J, Eyck GA, Wendt J R, Pluym T, Lilly M P, Coish W A, Pioro-Ladriére M and Carroll M S 2017 arXiv: 1703.02651v1 [cond-mat]

[56] Fogarty M A, Chan K W, Hensen B, Huang W, Tanttu T, Yang C H, Laucht A, Veldhorst M, Hudson F E, Itoh K M, Culcer D, Morello A and Dzurak A S 2017 arXiv: 1708.03445v1 [quant-ph]

[57] Chen B B, Wang B C, Cao G, Li H O, Xiao M and Guo G P 2017 *Sci. Bull.* **62** 712

[58] Laird E A, Taylor J M, DiVincenzo D P, Marcus C M, Hanson M P and Gossard A C 2010 *Phys. Rev. B* **82** 075403

[59] Taylor J M, Srinivasa V and Medford J 2013 *Phys. Rev. Lett.* **111** 050502

[60] Medford J, Beil J, Taylor J M, Bartlett S D, Doherty A C, Rashba E I, DiVincenzo D P, Lu H, Gossard A C and Marcus C M 2013 *Nat. Nanotechnol.* **8** 654

[61] Eng K, Ladd T D, Smith A, Borselli M G, Kiselev A A, Fong B H, Holabird K S, Hazard T M, Huang B, Deelman P W, Milosavljevic I, Schmitz A E, Ross R S, Gyure M F and Hunter A T 2015 *Sci. Adv.* **1** e1500214

[62] Reed M D, Maune B M, Andrews R W, Borselli M G, Eng K, Jura M P, Kiselev A A, Ladd T D, Merkel S T, Milosavljevic I, Pritchett E J, Rakher M T, Ross R S, Schmitz A E, Smith A, Wright J A, Gyure M F and Hunter A T 2016 *Phys. Rev. Lett.* **116** 110402

[63] Martins F, Malinowski F K, Nissen P D, Barnes E, Fallahi S, Gardner G C, Manfra M J, Marcus C M and Kuemmeth F 2016 *Phys. Rev. Lett.* **116** 116801

[64] Medford J, Beil J, Taylor J M, Rashba E I, Lu H, Gossard A C and Marcus C M 2013 *Phys. Rev. Lett.* **111** 050501

[65] Srinivasa V, Taylor JM and Tahan C 2016 *Phys. Rev. B* **94** 205421

[66] Landig A J, Koski J V, Scarlino P, Mendes U C, Blais A, Reichl C, Wegscheider W, Wallraff A, Ensslin K and Ihn T 2017 arXiv: 1711.01932v1 [cond-mat]

[67] Shi Z, Simmons C B, Prance J R, Gamble J K, Koh T S, Shim Y P, Hu X, Savage D E, Lagally M G, Eriksson M A, Friesen M and Coppersmith S N 2012 *Phys. Rev. Lett.* **108** 140503

[68] Shi Z, Simmons C B, Ward D R, Prance J R, Wu X, Koh T S, Gamble J K, Savage D E, Lagally M G, Friesen M, Coppersmith S N and Eriksson M A 2013 *Nat. Commun.* **5** 3020

[69] Koh T S, Gamble J K, Friesen M, Eriksson M A and Coppersmith S N 2012 *Phys. Rev. Lett.* **109** 250503

[70] Russ M and Burkard G 2016 arXiv: 1611.09106v1 [cond-mat]

[71] Kim D, Ward D R, Simmons C B, Savage D E, Lagally M G, Friesen M, Coppersmith S N and Eriksson M A 2015 *NPJ Quantum Inf.* **1** 15004

[72] Cao G, Li H O, Yu G D, Wang B C, Chen B B, Song X X, Xiao M, Guo G C, Jiang H W, Hu X and Guo G P 2016 *Phys. Rev. Lett.* **116** 086801

[73] Terhal B M 2015 *Rev. Mod. Phys.* **87** 307

[74] Fowler A G, Mariantoni M, Martinis J M and Cleland A N 2012 *Phys. Rev. A* **86** 032324

[75] Delbecq M R, Bruhat L E, Viennot J J, Datta S, Cottet A and Kontos T 2013 *Nat. Commun.* **4** 1400

[76] Frey T, Leek P J, Beck M, Blais A, Ihn T, Ensslin K and Wallraff A 2012 *Phys. Rev. Lett.* **108** 046807

[77] Petersson K D, McFaul L W, Schroer M D, Jung M, Taylor J M, Houck A A and Petta J R 2012 *Nature* **490** 380

[78] Han T Y, Deng G W, Wei D and Guo G P 2016 *Chin. Phys. Lett.* **33** 047301

[79] Deng G W, Wei D, Li S X, Johansson J R, Kong W C, Li H O, Cao G, Xiao M, Guo G C, Nori F and Jiang H W 2015 *Nano Lett.* **15** 6620

[80] Deng G W, Wei D, Johansson J R, Zhang M L, Li S X, Li H O, Cao G, Xiao M, Tu T, Guo G C and Jiang H W 2015 *Phys. Rev. Lett.* **115** 126804

[81] Stockklauser A, Scarlino P, Koski J V, Gasparinetti S, Andersen C K, Reichl C, Wegscheider W, Ihn T, Ensslin K and Wallraff A 2017 *Phys. Rev. X* **7** 011030

[82] Scarlino P, van Woerkom D J, Stockklauser A, Koski J V, Collodo M C, Gasparinetti S, Reichl C, Wegscheider W, Ihn T, Ensslin K and Wallraff A 2017 arXiv: 1711.01906v1 [quant-ph]

[83] Mi X, Cady J V, Zajac D M, Deelman P W and Petta J R 2017 *Science* **355** 156

[84] Mi X, Cady J V, Zajac D M, Stehlik J, Edge L F and Petta J R 2017 *Appl. Phys. Lett.* **110** 043502

[85] Bruhat L E, Cubaynes T, Viennot J J, Dartiailh M C, Desjardins M M, Cottet A and Kontos T 2016 arXiv: 1612.05214v1 [cond-mat]

[86] Viennot J J, Delbecq M R, Bruhat L E, Dartiailh M C, Desjardins M M, Baillergeau M, Cottet A and Kontos T 2016 *C. R. Phys.* **17** 705

[87] Viennot J J, Dartiailh M C, Cottet A and Kontos T 2015 *Science* **349** 408

[88] Mi X, Benito M, Putz S, Zajac D M, Taylor J M, Burkard G and Petta J R 2017 arXiv: 1710.03265v1 [cond-mat]

[89] Samkharadze N, Zheng G, Kalhor N, Brousse D, Sammak A, Mendes U C, Blais A, Scappucci G and Vandersypen L M K 2017 arXiv: 1711.02040v1 [cond-mat]

[90] McNeil R P, Kataoka M, Ford C J, Barnes C H, Anderson D, Jones G A, Farrer I and Ritchie D A 2011 *Nature* **477** 439

[91] Hermelin S, Takada S, Yamamoto M, Tarucha S, Wieck AD, Saminadayar L, Bäuerle C and Meunier T 2011 *Nature* **477** 435

[92] Braakman F R, Barthelemy P, Reichl C, Wegscheider W and Vandersypen L M K 2013 *Nat. Nanotechnol.* **8** 432

[93] Yamamoto M, Takada S, Bäuerle C, Watanabe K, Wieck A D and Tarucha S 2012 *Nat. Nanotechnol.* **7** 247

[94] Kyriakidis J and Burkard G 2007 *Phys. Rev. B* **75** 115324

[95] Shim Y P and Tahan C 2016 *Phys. Rev. B* **93** 121410

[96] Wang B C, Cao G, Li H O, Xiao M, Guo G C, Hu X, Jiang H W and Guo G P 2017 arXiv: 1706.03674v1 [cond-mat]

[97] Chen B B, Wang B C, Cao G, Li H O, Xiao M, Guo G C, Jiang H W, Hu X and Guo G P 2017 *Phys. Rev. B* **95** 035408

[98] Jones C, Gyure M F, Ladd T D, Fogarty M A, Morello A and Dzurak A S 2016 arXiv: 1608.06335v2 [quant-ph]

[99] Ruskov R, Veldhorst M, Dzurak A S and Tahan C 2017 arXiv: 1708.04555v1 [cond-mat]

[100] Colless J I, Mahoney A C, Hornibrook J M, Doherty A C, Lu H, Gossard A C and Reilly D J 2013 *Phys. Rev. Lett.* **110** 046805

[101] Hornibrook J M, Colless J I, Mahoney A C, Croot X G, Blanvillain S, Lu H, Gossard A C and Reilly D J 2014 *Appl. Phys. Lett.* **104** 103108

[102] Gonzalez-Zalba M F, Barraud S, Ferguson A J and Betz A C 2015 *Nat. Commun.* **6** 6084

[103] Crippa A, Maurand R, Kotekar-Patil D, Corna A, Bohuslavskyi H, Orlov A O, Fay P, Laviéville R, Barraud S, Vinet M, Sanquer M, Franceschi S D and Jehl X 2017 *Nano Lett.* **17** 1001

[104] Han T Y, Chen M B, Cao G, Li H O, Xiao M and Guo G P 2017 *Sci. China-Phys. Mech. Astron.* **60** 057301

[105] Thorgrimsson B, Kim D, Yang Y C, Simmons C B, Ward D R, Foote R H, Savage D E, Lagally M G, Friesen M, Coppersmith S N and Eriksson M A 2016 arXiv: 1611.04945v4 [cond-mat]

[106] Veldhorst M, Eenink H G J, Yang C H and Dzurak A S 2017 *Nat. Commun.* **8** 1766

[107] Vandersypen L M K, Bluhm H, Clarke J S, Dzurak A S, Ishihara R, Morello A, Reilly D J, Schreiber L R and Veldhorst M 2017 *NPJ Quantum Inf.* **3** 34

[108] Rotta D, Sebastiano F, Charbon E and Prati E 2017 *NPJ Quantum Inf.* **3** 26

[109] Li R, Petit L, Franke D P, Dehollain J P, Helsen J, Steudtner M, Thomas N K, Yoscovits Z R, Singh K J, Wehner S, Vandersypen L M K, Clarke J S and Veldhorst M 2017 arXiv: 1711.03807v1 [quant-ph]